

Higgscitement: Cosmological Dynamics of Fine Tuning

Mustafa A. Amin,¹ JiJi Fan,² Kaloian D. Lozanov,³ and Matthew Reece⁴

¹*Physics & Astronomy Department, Rice University, Houston, Texas 77005, USA*

²*Department of Physics, Brown University, Providence, RI, 02912, USA*

³*Max Planck Institute for Astrophysics, Karl-Schwarzschild-Str. 1, 85748 Garching, Germany*

⁴*Department of Physics, Harvard University, Cambridge, MA, 02138, USA*

The Higgs potential appears to be fine-tuned, hence very sensitive to values of other scalar fields that couple to the Higgs. We show that this feature can lead to a new epoch in the early universe featuring violent dynamics coupling the Higgs to a scalar modulus. The oscillating modulus drives tachyonic Higgs particle production. We find a simple parametric understanding of when this process can lead to rapid modulus fragmentation, resulting in gravitational wave production. A nontrivial equation-of-state arising from the nonlinear dynamics also affects the time elapsed from inflation to the CMB, influencing fits of inflationary models. Supersymmetric theories automatically contain useful ingredients for this picture.

I Introduction The origin of the Higgs mass and the mechanism of electroweak symmetry breaking (EWSB) are among the biggest puzzles in fundamental physics. Traditionally, it is expected that the answer lies in a natural new physics scenario with new particles proliferating around the TeV scale. Current data collected at the Large Hadron Collider (LHC) has put this traditional approach under considerable pressure. While active research aims to fill loopholes in LHC searches or to develop new natural models, it is also worthwhile to change our viewpoint. Suppose that the Higgs potential *is* tuned; how would we know? Searches for deviations in Higgs couplings or signals of new particles at the LHC are negative tests of fine tuning, that is, we infer tuning if we *fail* to find new physics. Our question is instead: is there a positive and direct way to probe tuning?

Fine tuning means that the Higgs potential is exquisitely sensitive to the physical constants of the Standard Model (SM). If they took different values, the Higgs mass term would either be large and positive (electroweak symmetry is unbroken) or large and negative (very badly broken). In this case, the universe is precariously balanced between no EWSB and severe EWSB. It is difficult to directly test this possibility, because physical constants have fixed values in our universe.

In the context of cosmology, however, it becomes possible to probe fine tuning. SM parameters are unlikely to be truly constant but are determined by the values of scalar fields.¹ In a tuned universe, even a small displacement of such a scalar field from its minimum can dramatically alter electroweak physics. In supersymmetric theories such scalars abound: moduli, saxions, and D-flat directions are naturally light fields with large expectation values. These fields have couplings to the SM suppressed by a large scale (e.g., the Planck scale), so they cannot be produced or detected at colliders. In the early universe, on the other hand, their very large and

time-dependent field values could dramatically affect the evolution of SM fields and the expansion rate of the universe.²

In this article, we initiate a study of the cosmology of fine-tuned electroweak symmetry breaking. As a proof of concept, we focus on a simple model in which the Higgs field is coupled to a modulus (which could be, but need not be, the inflaton) through a trilinear coupling (Fig. 1). If the universe is tuned, as the modulus field flips sign during its oscillation in the early universe, the effective Higgs mass term can flip from very large and positive to very large and negative. This could lead to non-adiabatic, out-of-equilibrium particle production with possible interesting consequences, such as a generation of gravitational waves and a change in the post-inflationary expansion history.

This article serves as the first step to explore the cosmological signals of Higgs fine tuning.³ It intends to open a new angle on the possible connection between

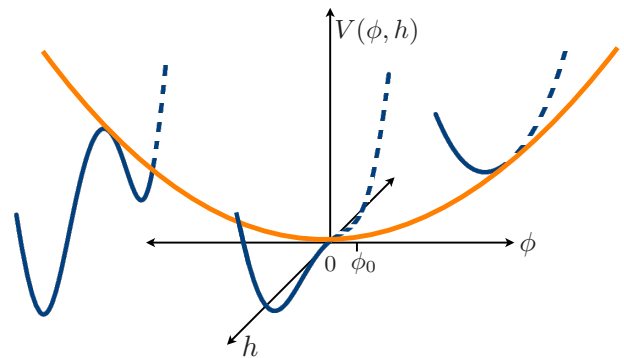


FIG. 1. The shape of the Higgs-moduli potential. Note that for $\phi = 0$, the Higgs can be in the (weakly) broken phase.

¹ Recent studies of time-dependent SM parameters in the early universe include [1–6].

² Earlier studies *not* focused on fine-tuned theories have suggested parametric resonance can solve the moduli problem [7] or not [8].

³ A different possible inflationary probe of fine-tuning is studied in [9].

electroweak symmetry breaking and early universe cosmology. It also motivates further studies on the potential of gravitational wave probes for new physics beyond the SM.

II A Simple Model A simplified potential capturing the most salient features of a Higgs field, h , coupled to a modulus, ϕ , is

$$\frac{1}{2}m_\phi^2\phi^2 + \frac{M^2}{f}(\phi - \phi_0)\left(h^\dagger h - \frac{v^2}{2}\right) + \lambda(h^\dagger h)^2. \quad (1)$$

The global minimum of the potential lies at $\phi = 0$, where the potential becomes simply the Standard Model Higgs potential. The constant $v^2 = M^2\phi_0/(\lambda f)$. Placing the minimum at $\phi = 0$ is a pure convention; in particular, ϕ carries no charges and can be shifted by a constant. We take the mass scale M^2 to be the natural value of the Higgs mass and f to be the natural scale of the modulus field ϕ . That is, we suppose that quantum corrections to the Higgs mass would be of order M^2 and that generic values $\phi \sim f$ produce Higgs masses of this order.

The effective Higgs boson mass

$$m_{h;\text{eff}}^2(\phi) = M^2\frac{\phi - \phi_0}{f} \quad (2)$$

is positive at $\phi \gg 0$ and negative at $\phi \ll 0$, transitioning through zero when $\phi = \phi_0$. The SM Higgs mass parameter is $m_{h;\text{eff}}^2(0) = -M^2\phi_0/f$. In this model, the criterion for fine tuning is

$$\text{Fine tuning} \Leftrightarrow \Delta \equiv \frac{f}{\phi_0} \gg 1. \quad (3)$$

In other words, it is an accident if the Higgs mass is zero at the same point where the ϕ potential is minimized; the closer these two points, the more surprising the result.

We will mostly have in mind supersymmetric theories, where this toy simplified potential can arise with $M^2 \sim m_{\text{sft}}^2$ as explained in §S4.2. We consider the hierarchy $|m_{h;\text{eff}}^2(0)| \ll m_\phi^2 \lesssim M^2 \ll f^2$. Terms we have neglected, such as $(m_\phi^2/f^2)\phi^4$ or $\frac{1}{f^2}\phi^2\partial_\mu\phi\partial^\mu\phi$, could have important effects on the dynamics (such as oscillon formation [10–14]). We assume that the field ϕ stays far from singular points in field space for all relevant times. For now we have omitted all modulus self-interactions for simplicity.

III Non-linear Dynamics In a *tuned* universe, the modulus-Higgs field system can undergo explosive, non-perturbative field dynamics leading to fragmentation of the fields on short time scales ($t \ll H^{-1}$), and yield a non-trivial equation of state for a number of e -folds of expansion following the fragmentation.

For $\Delta \gg 1$, the effective Higgs mass term oscillates between very large positive and negative values due to the oscillation of ϕ . One expects such oscillations to

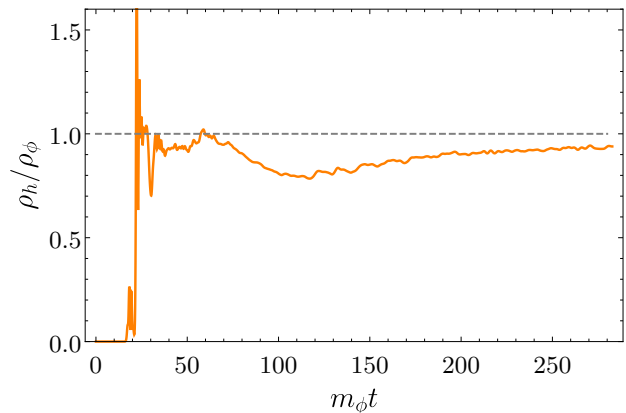


FIG. 2. The ratio of the spatially averaged energy density in the Higgs and modulus fields as a function of time obtained from our lattice simulations. This dynamics of energy transfer between the modulus and Higgs fields is representative of the case where the modulus fragments, i.e. when $b \equiv M^4/2\lambda f^2 m_\phi^2 \rightarrow 1$. For the above plot we have chosen $b = 1$, $M^2/m_\phi^2 = 10^2$ and $M/f = 10^{-12}$. The interaction term is not included in the above energy densities.

lead to non-adiabatic, out-of-equilibrium production of the Higgs particles. By considering tachyonic resonance [15], and for $f \sim \phi_{\text{in}} \sim m_{\text{pl}}$, the efficiency of such particle production is controlled by $q \equiv M^2/m_\phi^2$. In particular, $q \gg 1$ (as we assume) should lead to a broad range of physical momenta for the produced Higgs particles (see Fig. S3 in §S1).

Efficient transfer of energy from the modulus to the Higgs field is countered by the Higgs self-interaction λ . Large self-interactions block Higgs production, whereas at small λ the Higgs field will be sufficiently populated in non-zero momentum modes to backreact on the modulus, yielding a spatially inhomogeneous modulus (fragmentation). A more detailed view of the dynamics of the modulus-Higgs system can be seen in Fig. S2 in §S1.

A Does the modulus fragment? The Higgs field must be significantly populated in order to backreact on the modulus and cause its fragmentation. Large q favors tachyonic resonance whereas large λ limits the Higgs field occupation numbers. We define the fragmentation efficiency parameter

$$b \equiv \frac{M^4}{2\lambda f^2 m_\phi^2}, \quad (4)$$

which incorporates both effects to determine whether the modulus field fragments. Note that $b \leq 1$ from the constraint that the combined modulus-Higgs potential is positive definite. From detailed numerical simulations

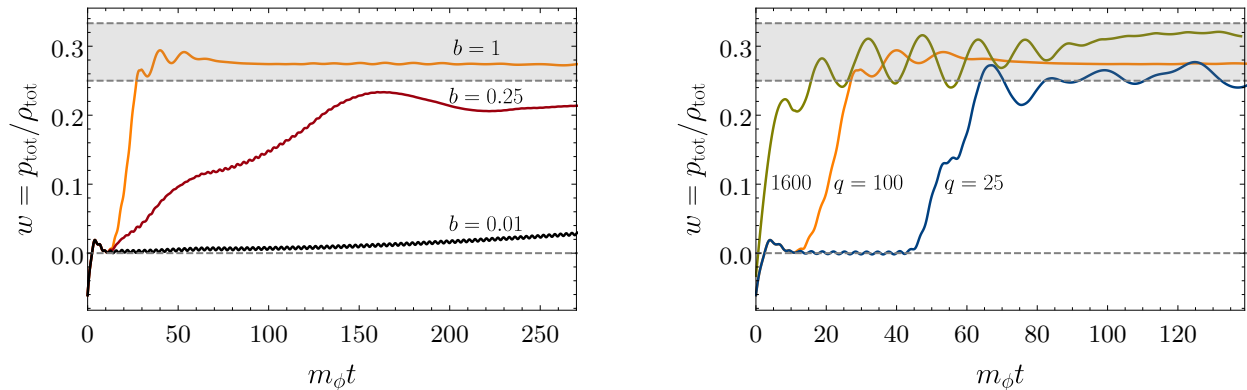


FIG. 3. Left Panel: Evolution of the equation of state of the universe for the Higgs-modulus system for different values of the fragmentation efficiency parameter $b \equiv M^4/2\lambda f^2 m_\phi^2$. An equation of state close to $1/4 \lesssim w \lesssim 1/3$ is attained for $b \rightarrow 1$ after fragmentation (orange curve). Smaller b yields smaller late time equations of state, with continued adiabatic evolution. Right Panel: When $b \rightarrow 1$, but we make different choices for $q = M^2/m_\phi^2$, we still get $1/4 \lesssim w \lesssim 1/3$ after fragmentation. The parameter q predominantly controls the speed with which $1/4 \lesssim w \lesssim 1/3$ is attained; q only affects the late time w value weakly when $b = 1$. For all curves, we have averaged the energy densities and pressures both spatially over the simulation box and temporally over fast oscillations.

(see §S1),⁴ we see no rapid fragmentation of the modulus field for $b \ll 1$ (as expected). For $b \rightarrow 1$, the modulus becomes completely fragmented, i.e. the energy density in the zero mode of the modulus is comparable to that in high-momentum modes. We find that for the duration of our simulations after fragmentation, $\rho_h/\rho_\phi \sim 1$ (see Fig. 2). That is, we are always left with significant energy density in the spatially inhomogeneous remnant modulus field.

B The Equation of State The expansion history of an FRW universe is controlled by the equation-of-state parameter w :

$$w \equiv \langle p_{\text{tot}} \rangle / \langle \rho_{\text{tot}} \rangle, \quad (5)$$

where $\langle \dots \rangle$ indicates spatial averaging over H^{-1} scales and temporal averaging over rapid oscillations in p_{tot} (due to oscillating fields). For fixed b , the detailed dynamics of the fields and time scale of fragmentation can depend on the particular values of q and λ . For example, for $b \rightarrow 1$, as q increases, the duration for the moduli to fragment decreases. However, w shows a simpler behavior as a function of b :

- For $b \rightarrow 1$, once the fields have fragmented, we get $1/4 \lesssim w \lesssim 1/3$ for the duration of our simulations ($\sim \text{few } e\text{-folds}$).⁵

- For $b \lesssim 1$, we find that a non-trivial ($0 < w < 1/3$), adiabatically evolving equation of state.
- For $b \ll 1$, $w \rightarrow 0$. Again, we see some adiabatic evolution of w here.

In the left panel of Fig. 3 we show the time evolution of w for a few representative b values. When we fixed $b = 1$ and changed q (along with λ), $1/4 \lesssim w \lesssim 1/3$ remained robust for late times in our simulations (right panel of Fig. 3).

C Very Long-term Dynamics: Beyond Simulations We do not have a clear understanding of the long-term evolution of this highly nonlinear system. Nevertheless, we venture some estimates of what we expect to happen. Even with complete fragmentation and an equation of state $w \sim 1/3$ seen in our simulations, there is significant energy density in the modulus field. We expect that after waiting long enough, the universe will again become matter dominated (unless additional physics is included).

Perturbative modulus decays occur on a timescale $\Gamma^{-1} \sim (m_{\text{pl}}/m_\phi)^2 m_\phi^{-1} \gg m_\phi^{-1}$, typically much longer than the duration of the simulations ($t_{\text{sim}} \sim \text{few} \times 10^2 m_\phi^{-1}$). Energy could be drained more quickly from the modulus if the Higgs decays to other light species, freeing up phase space for further moduli conversion into the Higgs field. We find it plausible that this might significantly reduce the energy density of the modulus compared to the decay products, though we have not simulated such dynamics. Nevertheless, it is difficult to see how matter domination can be avoided if even a small fraction of the initial energy density of the modulus survives in low momentum modes. In general we can allow

⁴ For simplicity, we substitute the complex h field by a real scalar field in the simulations.

⁵ Our result is mostly consistent with that of [15] where a similar system is studied in the post-inflationary preheating context.

a long-time averaged, constant $0 < w_{\text{mod}} < 1/3$ to stand in for a range of possible behaviors (including the possibility of a nontrivial ($w \neq 0, 1/3$) equation of state being maintained via nonlinear mode-mode couplings [15]).

IV Potential Signals and Consequences

A Stochastic Gravitational Waves As we have seen for $b \rightarrow 1$, the fields in the modulus-Higgs system fragment rapidly (for $q \gg 1$), thus providing a source for the production of gravitational radiation [16–19]. The characteristic physical frequency of gravitational waves at the time of their production is estimated to be $f \sim \beta^{-1} H_{\text{osc}}$, with $\beta \sim q^{-1/2}$ and $H_{\text{osc}} \sim m_\phi$ the Hubble parameter when the modulus starts oscillating. The frequency f at that time is then redshifted to today to obtain (see §S2 for details)

$$f_0 \sim \frac{a_{\text{osc}}}{a_0} \beta^{-1} H_{\text{osc}} \sim 10^5 \beta^{-1} \text{ Hz} \left(\frac{m_\phi}{10^5 \text{ TeV}} \right)^{1/2}, \quad (6)$$

where we assume that the universe can be approximated as radiation dominated shortly after ϕ begins oscillation. Note that for $\beta \ll 1$, these frequencies are beyond the reach of current interferometric detectors ($f \lesssim 10^3 \text{ Hz}$). However, techniques for probing higher frequencies in the future have been discussed [20–22].

The fraction of energy density in gravitational waves today (per logarithmic interval in frequency around f_0) can be estimated as [23]

$$\Omega_{\text{gw},0}(f_0) \sim \Omega_{\text{r},0} \delta_\pi^2 \beta^2, \quad (7)$$

where $\Omega_{\text{r},0}$ is today’s fraction of energy density stored in radiation and δ_π is the fraction of the energy density in anisotropic stresses at the time of gravitational wave production. From the scalar field simulations (or estimated from linear instability calculations and energetic arguments), $\delta_\pi \sim 0.3$ and $\beta \sim q^{-1/2}$ which yield $\Omega_{\text{gw},0} \sim 10^{-8}$ for $q = 10^2$. This result is consistent with our more detailed lattice simulations which calculate the gravitational wave spectrum using HLattice [24] (see Fig. 4). Note that detectable $\Omega_{\text{gw},0}(f_0 \sim 10^2 \text{ Hz}) \gtrsim 10^{-8}$ for aLIGO at design sensitivity [25].

We can relax the assumption of a radiation-like equation of state immediately after fragmentation and generalize the above formulae. Assuming that (i) fragmentation and gravitational wave production happens quickly after the modulus domination, (ii) the appropriately averaged equation of state $w = w_{\text{mod}}$ for N_{mod} e -folds after fragmentation and before final radiation domination kicks in, we get the following generalization of the above formulae (see §S2 for details)

$$f_0 \sim e^{-\frac{N_{\text{mod}}(1-3w_{\text{mod}})}{4}} \left(\frac{m_\phi}{10^5 \text{ TeV}} \right)^{1/2} 10^5 \beta^{-1} \text{ Hz}$$

$$\Omega_{\text{gw},0}(f_0) \sim e^{-N_{\text{mod}}(1-3w_{\text{mod}})} \Omega_{\text{r},0} \delta_\pi^2 \beta^2 \quad (8)$$

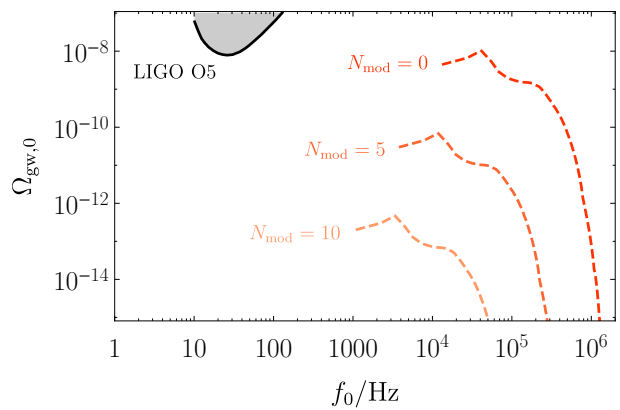


FIG. 4. The dashed orange curve with $N_{\text{mod}} = 0$ is the gravitational waves (GWs) power spectrum today; it was generated by the non-linear dynamics at $t \approx 70 m_\phi^{-1}$ (we assume $b = 1, q = 10^2, f = m_{\text{pl}}$). The height and the frequency of the peak are consistent with our predictions. The GWs at intermediate frequencies are generated by the slow propagation of power towards smaller comoving scales after backreaction, see Fig. S3. The two paler dashed orange curves with $N_{\text{mod}} > 0$ are just a rescaled version of the top one, assuming $w_{\text{mod}} = 0$. The solid black curve is the planned sensitivity of the fifth observational run, O5, of the aLIGO-AdVirgo detector collaboration [26].

Note that a more observationally accessible, lower frequency signal using large values of $N_{\text{mod}}(1 - 3w_{\text{mod}})$ would lead to a significant suppression of $\Omega_{\text{gw},0}$, making detection challenging.

B Constraints from/on Inflationary Observables

Another possible consequence of the non-linear dynamics is to change the allowed e -folds during inflation. The e -folds between the time the current co-moving horizon scale exited the horizon during inflation and the end of inflation are related to the e -folds between the end of inflation and today in a given expansion history [27]. The expansion history also allows us to keep track of the evolution of the energy density. Then the n_s and r bounds from CMB measurements constrain an inflationary model together with its associated evolution afterwards. The co-moving Hubble scale $k = a_k H_k$ that exits the horizon during inflation could be written as

$$k = a_k H_k = \frac{a_k}{a_{\text{end}}} \frac{a_{\text{end}}}{a_{\text{re}}} \frac{a_{\text{re}}}{a_{\text{mod}}} \frac{a_{\text{mod}}}{a_{\text{dec}}} a_{\text{dec}} H_k, \quad (9)$$

where $a_{\text{end}}, a_{\text{re}}, a_{\text{mod}}, a_{\text{dec}}$ are the scale factors at the end of inflation, at the end of inflationary reheating, when the modulus starts to oscillate, and when full decays of the modulus happen (equivalently when radiation dominates again) respectively. Using this relation and assuming that during inflationary reheating, the constant in the equation of state doesn’t exceed $1/3$, we can obtain

a conservative lower bound on m_ϕ ,

$$\frac{m_\phi^2}{m_{\text{pl}}^2} \gtrsim \exp \left[\frac{-6(1+w_{\text{mod}})}{1-3w_{\text{mod}}} \left(57 - N_k + \ln \left(\frac{r\rho_k}{\rho_{\text{end}}} \right)^{\frac{1}{4}} \right) \right]$$

where r is the tensor-to-scalar ratio and ρ_k (ρ_{end}) is the energy density when the mode exits the horizon (at the end of inflation). For $0 < w_{\text{mod}} < 1/3$, the bound can be considerably weaker compared to the $w_{\text{mod}} = 0$ case. Details of the derivation and more discussions on the implications of this bound can be found in §S3.

V More Realistic Models The simulation establishes that the relation $M^4 \sim \lambda m_\phi^2 f^2$ is crucial for fragmentation. In a gravity-mediated SUSY scenario, we expect $M \sim m_\phi \sim m_{\text{soft}} \ll f \sim m_{\text{pl}}$ with m_{soft} the SUSY breaking soft mass. Modulus fragmentation then requires a tiny Higgs quartic coupling $\lambda \sim m_{\text{soft}}^2/m_{\text{pl}}^2$, at first glance conflicting with the known SM Higgs mass. However, in the SUSY context with two Higgs doublets, there is a D -flat direction $|h_u| \approx |h_d|$ along which the effective quartic coupling can be tiny. If, as the modulus oscillates, the D -flat direction becomes tachyonic, we could achieve $b \sim 1$.

Loop corrections lifting the D -flat direction are tiny at large Higgs VEV, e.g. $\propto \log \left(1 + \frac{m_{\text{soft}}^2}{y_t^2 \langle h \rangle^2} \right)$. Higher dimension operators involving a SUSY breaking spurion X produce effective quartic couplings

$$\int d^4\theta \frac{\mathbf{X}^\dagger \mathbf{X}}{\Lambda^4} (h_u^\dagger h_u)^2 \rightarrow \frac{m_{\text{soft}}^2}{\Lambda^2} (h_u^\dagger h_u)^2, \quad (10)$$

precisely the right size to achieve $b \sim 1$ if the cutoff $\Lambda \sim m_{\text{pl}}$. More details are in §S4.

We could consider alternative scale hierarchies, e.g. $m_\phi \ll M \ll f \sim m_{\text{pl}}$ while keeping the Higgs quartic coupling order one. This requires sequestering SUSY breaking to the modulus compared to the Higgs field. We will leave more detailed model building to future work.

VI Conclusions and Future Directions If the physical constants of the SM are determined by the vacuum expectation values of some scalar fields, in a tuned

universe, even a small displacement of such a scalar field from its minimum can dramatically alter electroweak physics, leading to highly non-trivial dynamics in the early universe. We demonstrate this simple idea in a modulus-Higgs system. We find that in the simplest model (eq. (1)), for $b = M^4/(2\lambda f^2 m_\phi^2) \rightarrow 1$, we get rapid fragmentation of the fields. This fragmentation leads to: (i) generation of gravitational waves; (ii) a non-trivial equation-of-state $1/4 \lesssim w \lesssim 1/3$ for the duration of the simulations. The non-trivial equation of state can lead to a change in constraints on inflationary models, or alternatively, change constraints on the moduli mass. Assuming an equation of state $w \approx 1/3$ is maintained (for example, through the decay of the Higgs) up to eventual matter domination at a_{eq} , we can expect a stochastic background of gravitational waves at high frequencies $f \gtrsim 10^5 \text{ Hz} \times \sqrt{m_\phi/(10^3 \text{ TeV})}$, with $\Omega_{\text{gw},0} \sim 10^{-8}$.

This paper only serves as the first step to explore the cosmological dynamics of electroweak fine tuning. Further numerical work could investigate how a more complete model affects the dynamics. Simulations should include the full two Higgs doublet model with a flat direction, as well as additional couplings. In many cases we expect that a modulus could fragment via its own self-couplings, forming oscillons. A fine-tuned Higgs could still play an important dynamical role by providing a novel oscillon decay mechanism.

Acknowledgments We thank Patrick Draper and David Pinner for discussions in early stages of this project, Marcos Garcia for feedback on the manuscript, and Eiichiro Komatsu and Rouzbeh Allahverdi for useful conversations. Part of the simulations were carried out on the COSMOS Shared Memory system at DAMTP, operated by U. of Cambridge on behalf of the STFC DiRAC HPC Facility. We thank D. Sijacki for her generosity regarding the use of her computational resources under the Cambridge COSMOS Consortium. For the rest of the simulations we used the facilities of the central computing center of the Max-Planck Society. This work was initiated at the Aspen Center for Physics, supported by National Science Foundation grant PHY-1607611. MA is supported by a DOE grant DE-SC0018216; JF by the DOE grant DE-SC0010010; MR by the NASA ATP Grant NNX16AI12G and by the DOE Grant DE-SC0013607.

-
- [1] R. Fardon, A. E. Nelson, and N. Weiner, *JCAP* **0410**, 005 (2004), [arXiv:astro-ph/0309800 \[astro-ph\]](#).
 [2] G. Servant, *Phys. Rev. Lett.* **113**, 171803 (2014), [arXiv:1407.0030 \[hep-ph\]](#).
 [3] P. W. Graham, D. E. Kaplan, and S. Rajendran, *Phys. Rev. Lett.* **115**, 221801 (2015), [arXiv:1504.07551 \[hep-ph\]](#).
 [4] Y. Ema, K. Mukaida, and K. Nakayama, *Phys. Lett.* **B761**, 419 (2016), [arXiv:1605.07342 \[hep-ph\]](#).
 [5] I. Baldes, T. Konstandin, and G. Servant, (2016), [arXiv:1604.04526 \[hep-ph\]](#).
 [6] B. von Harling and G. Servant, *JHEP* **05**, 077 (2017), [arXiv:1612.02447 \[hep-ph\]](#).
 [7] N. Shuhmaher and R. Brandenberger, *Phys. Rev.* **D73**, 043519 (2006), [arXiv:hep-th/0507103 \[hep-th\]](#).

- [8] J. T. Giblin, G. Kane, E. Nesbit, S. Watson, and Y. Zhao, *Phys. Rev.* **D96**, 043525 (2017), [arXiv:1706.08536 \[hep-th\]](#).
- [9] S. Kumar and R. Sundrum, (2017), [arXiv:1711.03988 \[hep-ph\]](#).
- [10] M. Gleiser, *Phys. Rev.* **D49**, 2978 (1994), [arXiv:hep-ph/9308279 \[hep-ph\]](#).
- [11] E. J. Copeland, M. Gleiser, and H. R. Muller, *Phys. Rev.* **D52**, 1920 (1995), [arXiv:hep-ph/9503217 \[hep-ph\]](#).
- [12] M. A. Amin, R. Easther, H. Finkel, R. Flauger, and M. P. Hertzberg, *Phys. Rev. Lett.* **108**, 241302 (2012), [arXiv:1106.3335 \[astro-ph.CO\]](#).
- [13] M. A. Amin, *Phys. Rev.* **D87**, 123505 (2013), [arXiv:1303.1102 \[astro-ph.CO\]](#).
- [14] S. Antusch, F. Cefala, S. Krippendorf, F. Muia, S. Orani, and F. Quevedo, *JHEP* **01**, 083 (2018), [arXiv:1708.08922 \[hep-th\]](#).
- [15] J. F. Dufaux, G. N. Felder, L. Kofman, M. Peloso, and D. Podolsky, *JCAP* **0607**, 006 (2006), [arXiv:hep-ph/0602144 \[hep-ph\]](#).
- [16] S. Y. Khlebnikov and I. I. Tkachev, *Phys. Rev.* **D56**, 653 (1997), [arXiv:hep-ph/9701423 \[hep-ph\]](#).
- [17] R. Easther and E. A. Lim, *JCAP* **0604**, 010 (2006), [arXiv:astro-ph/0601617 \[astro-ph\]](#).
- [18] J. F. Dufaux, A. Bergman, G. N. Felder, L. Kofman, and J.-P. Uzan, *Phys. Rev.* **D76**, 123517 (2007), [arXiv:0707.0875 \[astro-ph\]](#).
- [19] J. Garcia-Bellido and D. G. Figueroa, *Phys. Rev. Lett.* **98**, 061302 (2007), [arXiv:astro-ph/0701014 \[astro-ph\]](#).
- [20] T. Akutsu *et al.*, *Phys. Rev. Lett.* **101**, 101101 (2008), [arXiv:0803.4094 \[gr-qc\]](#).
- [21] M. Goryachev and M. E. Tobar, *Phys. Rev.* **D90**, 102005 (2014), [arXiv:1410.2334 \[gr-qc\]](#).
- [22] A. Arvanitaki and A. A. Geraci, *Phys. Rev. Lett.* **110**, 071105 (2013), [arXiv:1207.5320 \[gr-qc\]](#).
- [23] M. A. Amin, M. P. Hertzberg, D. I. Kaiser, and J. Karouby, *Int. J. Mod. Phys.* **D24**, 1530003 (2014), [arXiv:1410.3808 \[hep-ph\]](#).
- [24] Z. Huang, *Phys. Rev.* **D83**, 123509 (2011), [arXiv:1102.0227 \[astro-ph.CO\]](#).
- [25] B. P. Abbott *et al.* (Virgo, LIGO Scientific), *Phys. Rev. Lett.* **118**, 121101 (2017), [Erratum: *Phys. Rev. Lett.* **119**, no.2, 029901 (2017)], [arXiv:1612.02029 \[gr-qc\]](#).
- [26] B. P. Abbott *et al.* (Virgo, LIGO Scientific), *Phys. Rev. Lett.* **116**, 131102 (2016), [arXiv:1602.03847 \[gr-qc\]](#).
- [27] A. R. Liddle and S. M. Leach, *Phys. Rev.* **D68**, 103503 (2003), [arXiv:astro-ph/0305263 \[astro-ph\]](#).
- [28] G. N. Felder and I. Tkachev, *Comput. Phys. Commun.* **178**, 929 (2008), [arXiv:hep-ph/0011159 \[hep-ph\]](#).
- [29] J. T. Giblin and E. Thrane, *Phys. Rev.* **D90**, 107502 (2014), [arXiv:1410.4779 \[gr-qc\]](#).
- [30] P. A. R. Ade *et al.* (Planck), *Astron. Astrophys.* **594**, A20 (2016), [arXiv:1502.02114 \[astro-ph.CO\]](#).
- [31] J. Garcia-Bellido, D. G. Figueroa, and A. Sastre, *Phys. Rev.* **D77**, 043517 (2008), [arXiv:0707.0839 \[hep-ph\]](#).
- [32] R. Easther, R. Galvez, O. Ozsoy, and S. Watson, *Phys. Rev.* **D89**, 023522 (2014), [arXiv:1307.2453 \[hep-ph\]](#).
- [33] K. Dutta and A. Maharana, *Phys. Rev.* **D91**, 043503 (2015), [arXiv:1409.7037 \[hep-ph\]](#).
- [34] M. Cicoli, K. Dutta, A. Maharana, and F. Quevedo, *JCAP* **1608**, 006 (2016), [arXiv:1604.08512 \[hep-th\]](#).
- [35] K. N. Abazajian *et al.* (CMB-S4), (2016), [arXiv:1610.02743 \[astro-ph.CO\]](#).
- [36] M. Cicoli, J. P. Conlon, and F. Quevedo, *Phys. Rev.* **D87**, 043520 (2013), [arXiv:1208.3562 \[hep-ph\]](#).
- [37] T. Higaki and F. Takahashi, *JHEP* **11**, 125 (2012), [arXiv:1208.3563 \[hep-ph\]](#).
- [38] M. Reece and W. Xue, *JHEP* **04**, 045 (2016), [arXiv:1512.04941 \[hep-ph\]](#).
- [39] I. Affleck, M. Dine, and N. Seiberg, *Nucl. Phys.* **B241**, 493 (1984).
- [40] I. Affleck, M. Dine, and N. Seiberg, *Nucl. Phys.* **B256**, 557 (1985).
- [41] T. Gherghetta, C. F. Kolda, and S. P. Martin, *Nucl. Phys.* **B468**, 37 (1996), [arXiv:hep-ph/9510370 \[hep-ph\]](#).
- [42] I. Affleck and M. Dine, *Nucl. Phys.* **B249**, 361 (1985).
- [43] M. Dine, L. Randall, and S. D. Thomas, *Nucl. Phys.* **B458**, 291 (1996), [arXiv:hep-ph/9507453 \[hep-ph\]](#).
- [44] A. Brignole, L. E. Ibáñez, and C. Muñoz, *Phys. Lett.* **B387**, 769 (1996), [arXiv:hep-ph/9607405 \[hep-ph\]](#).
- [45] G. Burdman and Y. Nomura, *Nucl. Phys.* **B656**, 3 (2003), [arXiv:hep-ph/0210257 \[hep-ph\]](#).
- [46] K.-w. Choi, N.-y. Haba, K.-S. Jeong, K.-i. Okumura, Y. Shimizu, and M. Yamaguchi, *JHEP* **02**, 037 (2004), [arXiv:hep-ph/0312178 \[hep-ph\]](#).
- [47] G. R. Dvali and L. M. Krauss, (1998), [arXiv:hep-ph/9811298 \[hep-ph\]](#).
- [48] E. Witten, *Phys. Lett.* **105B**, 267 (1981).
- [49] G. F. Giudice and A. Masiero, *Phys. Lett.* **B206**, 480 (1988).
- [50] K. S. Babu, I. Gogoladze, and K. Wang, *Nucl. Phys.* **B660**, 322 (2003), [arXiv:hep-ph/0212245 \[hep-ph\]](#).
- [51] H. M. Lee, S. Raby, M. Ratz, G. G. Ross, R. Schieren, K. Schmidt-Hoberg, and P. K. S. Vaudrevange, *Nucl. Phys.* **B850**, 1 (2011), [arXiv:1102.3595 \[hep-ph\]](#).

Higgscitement: Cosmological Dynamics of Fine Tuning

Supplementary Material

Mustafa A. Amin, JiJi Fan, Kaloian D. Lozanov, and Matthew Reece

S1 Field Dynamics and Lattice Simulations

1. Equations of Motion and Initial Conditions

We work in a flat Friedmann-Robertson-Walker (FRW) universe with the metric

$$ds^2 = dt^2 - a^2(t)\delta_{ij}dx^i dx^j. \quad (\text{S1})$$

The dynamics of the modulus-Higgs system is determined by

$$\ddot{\phi} + 3H\dot{\phi} - \frac{\nabla^2}{a^2}\phi + \partial_\phi V(\phi, h) = 0, \quad \ddot{h} + 3H\dot{h} - \frac{\nabla^2}{a^2}h + \partial_h V(\phi, h) = 0, \quad (\text{S2})$$

where the potential is given by

$$V(\phi, h) = \frac{1}{2}m_\phi^2\phi^2 + \frac{1}{2}\frac{M^2}{f}\phi h^2 + \frac{1}{4}\lambda h^4. \quad (\text{S3})$$

Note that we assume that ϕ and h are two real scalar fields, representing the modulus and the Higgs, respectively. For simplicity we assume that the Higgs is a real scalar field here and ignore the Higgs vev also. Because ϕ_0 and v in the full potential (1) are small, we expect that they affect the dynamics significantly only at times much later than those that we simulate (once $\langle\phi\rangle$ has significantly redshifted). The Hubble parameter is determined via the Friedmann equation with $H^2 = (\dot{a}/a)^2 = \langle\rho_{\text{tot}}\rangle/3m_{\text{pl}}^2$ where $\langle\rho_{\text{tot}}\rangle$ is the spatially averaged, total energy density of the fields.

We note that for most of this section and the subsequent one on gravitational waves, we will provide results for the above toy model. Nevertheless, we will point out features that might be qualitatively different when considering the more realistic potential with a higher dimensional field space.

We assume that initially the modulus has a non-zero vacuum expectation value, $\phi_{\text{in}} \sim m_{\text{pl}}$ (where the Higgs has a positive mass), but that the Higgs does not, $h_{\text{in}} = 0$. The initial Hubble rate is (ignoring contributions from vacuum fluctuations)

$$H_{\text{in}} \approx \frac{\sqrt{V_{\text{in}}}}{\sqrt{3}m_{\text{pl}}} = \frac{m_\phi}{\sqrt{6}}. \quad (\text{S4})$$

Since the mass of the modulus is comparable to the Hubble rate, we expect the modulus to start oscillating right away.

Along with the homogeneous fields, vacuum fluctuations ($\delta\phi$ and δh) are present in the fields. The mode functions for the quantum fluctuations satisfy linearized equations around a time-dependent classical background determined by $\phi(t)$ and $a(t)$. Such a linear description typically suffices to capture the initial evolution of $\delta\phi$ and δh . If there are growing (i.e., unstable) modes, the linear description eventually becomes inaccurate and the occupation number of these fields becomes quite high. Hence, it is plausible that the subsequent non-linear evolution system can be studied classically with lattice simulations.

2. Linear instabilities in the Higgs

The linearized equations of motion for $\delta\phi$ and δh are

$$\delta\ddot{\phi} + 3H\delta\dot{\phi} - \frac{\nabla^2}{a^2}\delta\phi + m_\phi^2\delta\phi = 0, \quad (\text{S5})$$

$$\delta\ddot{h} + 3H\delta\dot{h} - \frac{\nabla^2}{a^2}\delta h + \frac{M^2}{f}\phi(t)\delta h = 0, \quad (\text{S6})$$

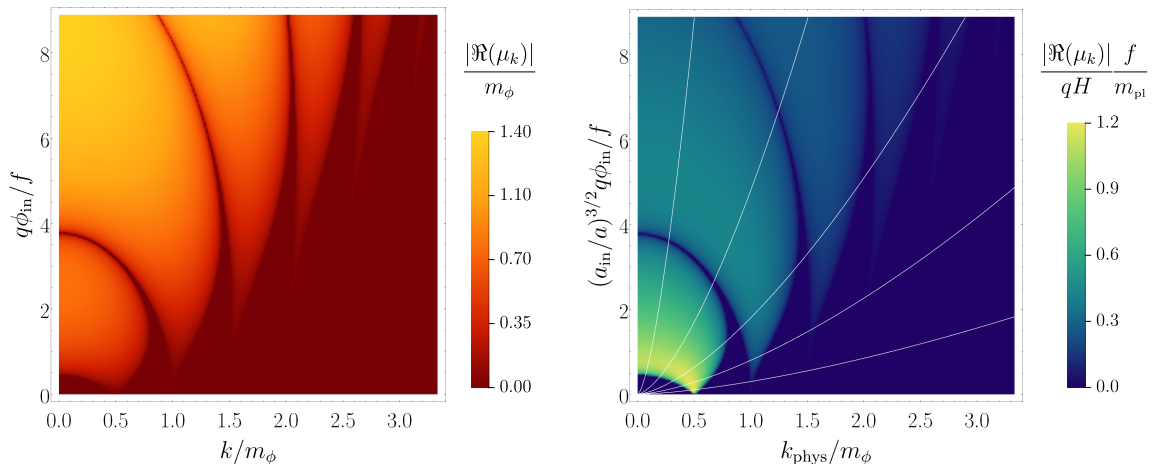


FIG. S1. The instability chart featuring the real part of the Floquet exponent normalized by the modulus mass (left) and the Hubble rate (right), characterizing the Higgs particle production rate. When $\phi_{\text{in}} \sim f$, Higgs particle production is expected for $q > 1$. In FRW space-time $k_{\text{phys}} = k/a(t)$, implying that a given co-moving mode flows towards the bottom left corner of the chart as the universe expands as indicated with the white lines in the second chart. Note that particle production is efficient if $|\Re(\mu_k)|/H \sim qm_{\text{pl}}/f \gg 1$.

implying that at the linear level the modulus fluctuations evolve as those of a scalar field with a constant mass, whereas the Higgs ones have a time-dependent mass which can lead to instabilities.

The Fourier modes of the canonically normalized Higgs, $\delta h_c = a^{3/2}\delta h$, evolve according to

$$\delta \ddot{h}_{ck} + \omega^2(k, t)\delta h_{ck} = 0, \quad (\text{S7})$$

where

$$\omega^2(k, t) = \frac{k^2}{a^2} + \frac{M^2}{f}\phi(t) - (3H/2)^2 - (3/2)\dot{H} \approx \frac{k^2}{a^2} + \frac{M^2}{f}\phi_{\text{in}} \left(\frac{a_{\text{in}}}{a(t)}\right)^{3/2} \cos(m_\phi t). \quad (\text{S8})$$

In the last line, we have used a standard approximation for a massive oscillating background scalar field, namely $a^{3/2}(t)\phi(t) \propto \cos(m_\phi t)$ and $3H^2 \approx -2\dot{H}$. For small enough k

$$\frac{k}{a(t)} = k_{\text{phys}} < m_\phi \sqrt{q \frac{\phi_{\text{in}}}{f} \left(\frac{a_{\text{in}}}{a(t)}\right)^{3/2}}, \quad (\text{S9})$$

This implies that $\omega^2(k, t) < 0$ for nearly a half of the $\phi(t)$ oscillation. Such co-moving modes can then be unstable, and grow exponentially with time. In the context of *preheating* this amplification is known as *tachyonic resonance*.

To study parametric resonance in the Higgs from a periodic frequency change, one can resort to Floquet theory. If we ignore expansion, i.e., put $a(t) = \text{const.}$ and $\phi(t) = \phi_{\text{in}} \cos(m_\phi t)$, then Eq. (S7) is just the equation of motion of a simple harmonic oscillator with a periodically varying angular frequency. The Floquet theorem then tells us that its solution takes the form

$$\delta h_{ck}(t) = e^{\mu_k t} \mathcal{P}_{k+}(t) + e^{-\mu_k t} \mathcal{P}_{k-}(t), \quad (\text{S10})$$

where μ_k is called the Floquet exponent and $\mathcal{P}_{k\pm}(t)$ are periodic functions of time. If $\Re(\mu_k) \neq 0$ one of the two terms increases exponentially with time. The numerically obtained exponent is given in the left panel in Fig. S1 as a function of the model parameters. The broad instability bands are consistent with our naive expectations, Eq. (S9). To explain the additional features, such as narrow stability and instability bands one has to consider the evolution of $\delta h_{ck}(t)$ in greater detail, e.g., take into account the non-adiabatic change of $\omega^2(k, t)$ every time $\phi(t) = 0$ for small enough k and large initial amplitudes.

However, these small features are irrelevant after the expansion of the universe is restored. In the right panel in Fig. S1 we show that a given co-moving mode can flow across multiple broad instability bands. If $|\Re(\mu_k)| \gg H$, the mode amplitude can grow significantly within less than an e -fold of expansion.

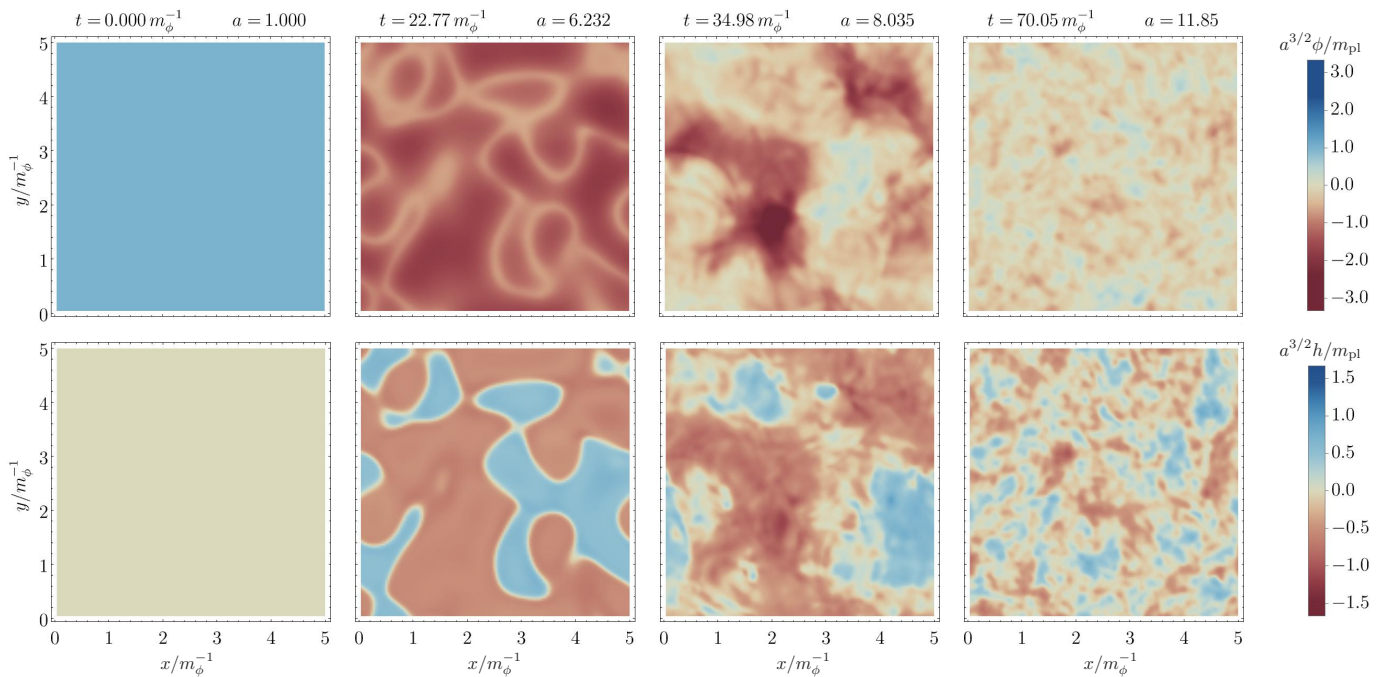


FIG. S2. Snapshots of the values of the modulus (first row) and Higgs (second row) fields on an arbitrary two-dimensional slice through the 3 dimensional simulation box at four different times (the spatial coordinates are co-moving). Around the time of backreaction, $t \approx 23m_\phi^{-1}$ (second column), the Higgs field forms domains (‘bubbles’) with $h = \pm\sqrt{2|\phi|f/q}$. They disappear within $\Delta t \sim 10m_\phi^{-1}$, due to collisions, as well as oscillations of the remnant ϕ condensate. The parameters we used are $b = 1$, $q = 10^2$, $M = 10^{-12}m_{\text{pl}}$, $f = m_{\text{pl}}$.

3. Important Parameters for the Nonlinear Dynamics

We have shown that the Higgs vacuum fluctuations can be linearly unstable and grow exponentially with time. As non-linear terms from the potential in Eq. (S3) become important, the exponential growth is expected to slow down. To estimate whether the energy in the amplified fluctuations is comparable to the background or not around the time non-linearities become significant we return to the *backreaction efficiency parameter*

$$b \equiv \frac{M^4}{2\lambda f^2 m_\phi^2} = \frac{1}{4} \left(\frac{\frac{1}{2} \frac{M^2}{f} \phi h^2}{\frac{1}{2} m_\phi^2 \phi^2} \right) \left(\frac{\frac{1}{2} \frac{M^2}{f} \phi h^2}{\frac{1}{4} \lambda h^4} \right) \leq 1. \quad (\text{S11})$$

Note $b \leq 1$ is required for $V \geq 0$.

If $b \ll 1$ and we assume that the energy in the amplified fluctuations is comparable to the background, i.e., $M^2 \phi h^2 / (2f) \sim m_\phi^2 \phi^2 / 2$, then $M^2 \phi h^2 / (2f) \ll \lambda h^4 / 4$. The latter inequality implies that the quartic Higgs self-interaction has become important much earlier. Therefore, the Higgs instability is shut down before the amplified Higgs fluctuations have become energetic enough to backreact on the modulus background. We are left with a strongly self-coupled Higgs, interacting relatively weakly with the energetically dominant $\phi(t)$. The modulus is expected to remain homogeneous for a very long time.

If $b \lesssim 1$ and we again assume that the energy in the amplified fluctuations is comparable to the background, i.e., $M^2 \phi h^2 / (2f) \sim m_\phi^2 \phi^2 / 2$, then $M^2 \phi h^2 / (2f) \lesssim \lambda h^4 / 4$. The latter inequality implies that the quartic Higgs self-interaction becomes important around the time the amplified Higgs fluctuations have become energetic enough to backreact on the modulus background. The ensuing non-linear dynamics leads to the rapid fragmentation of $\phi(t)$.

Another useful parameter that characterizes the nonlinear dynamics is $q \equiv M^2 / m_\phi^2$ which controls the speed of energy transfer from the modulus to the Higgs (see right panel in Fig. 3). For the purpose of numerical simulations and the discussion below, we set $M = 10^{-12}m_{\text{pl}}$, and treat b , q and f as parameters to vary. We have carried out simulations where we varied the parameters between $0.001 \leq b \leq 1$, $25 \leq q \leq 1600$ and $10^{-1} \leq f/m_{\text{pl}} \leq 1$.

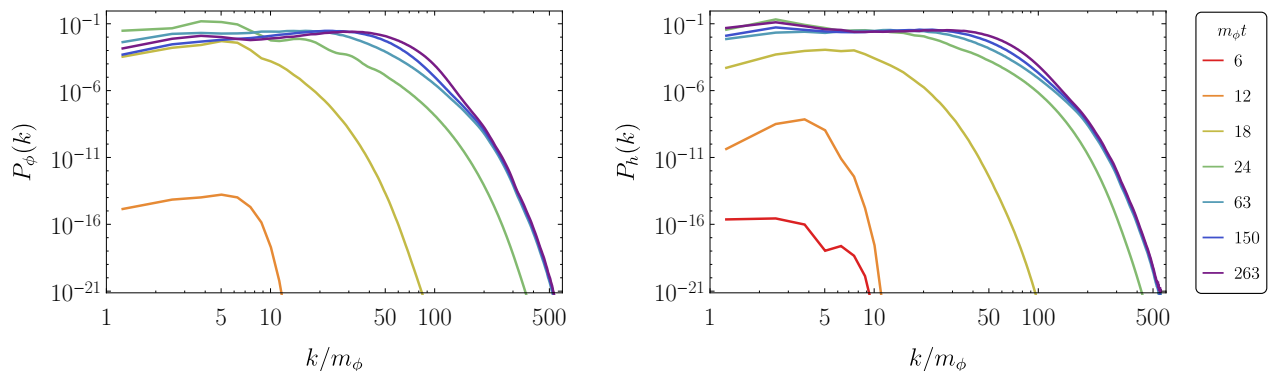


FIG. S3. The evolution of the normalized fields power spectra for the orange curve in Fig. 3 (with $b = 1, q = 10^2, f = m_{\text{pl}}$). The normalized power spectrum of a field $F(\mathbf{x})$ is $P_F(k) \equiv \phi_{\text{osc}}^{-2} (d/d \ln k) F^2(\mathbf{x})$, where ϕ_{osc} is the amplitude of the background modulus oscillations. For this normalization, when $P_\phi(k) = \mathcal{O}(1)$, the modulus becomes inhomogeneous. Initially, the tachyonic instability in the Higgs is closely followed by excitations in the modulus (due to re-scattering). Comoving modes $k < m_\phi q^{1/2}$ grow exponentially. At the third oscillation of the modulus backreaction takes place. The spectra then settle down and power slowly propagates towards higher comoving modes.

4. Lattice Simulations

We use the parallelized version of LatticeEasy [28] to calculate the non-linear evolution of the fields and the self-consistent evolution of $a(t)$. The initial physical length of the edge of the simulation box is $L_{\text{in}} = 0.5H_{\text{in}}^{-1} - 2.5H_{\text{in}}^{-1}$, whereas we set $a_{\text{in}} = 1$, with $a_{\text{end}} \sim \mathcal{O}[\text{few } e\text{-folds}]$. Note that a slightly super-horizon box was needed sometimes to capture the tachyonic instability in h . The number of co-moving lattice points is $N = 512^3$, and our time steps vary between $dt = 0.00125m_\phi^{-1}$ to $0.000625m_\phi^{-1}$ depending on the parameters chosen. The violation of the energy conservation in the above simulations is always less than $\mathcal{O}[10^{-4}]$.

At the start of the simulations ϕ has a background value, set to $\phi_{\text{in}} = m_{\text{pl}}$. The initial background field velocity, $\dot{\phi}_{\text{in}}$, is equal to $-3H_{\text{in}}\phi_{\text{in}}/2$, in accordance with LatticeEasy conventions. The initial Fourier modes of the fields and field velocities (excluding the zero modes of ϕ and $\dot{\phi}$) are drawn from Gaussian probability distributions with covariance matrices equal to the squared amplitudes of the corresponding vacuum fluctuations. Initially, the energy budget is dominated by the homogeneous ϕ , i.e., almost no energy is stored in the gradients. The values of ϕ_{in} and $\dot{\phi}_{\text{in}}$ imply that $w_{\text{in}} \approx -1/4$ which is equivalent to starting the simulation soon after the end of slow-roll inflation if ϕ was the inflaton.

Simulation Outputs: Snapshots of the evolution of Higgs and modulus fields are shown in Fig. S2. The modulus first begins its oscillations from $\phi_{\text{in}} = m_{\text{pl}}$, then passes through $\phi = 0$, causing the Higgs potential to develop minima. After a few oscillations, the fields start exploring these minima in a spatially inhomogeneous manner, leading to the formation of temporary domains. This is also the time when the backreaction on the oscillating modulus field becomes relevant. These domains quickly interact with each other and the still oscillating modulus field leading to complex spatio-temporal behaviour of the fields. The domains annihilate and the modulus field fragments spatially. The formation and dynamics of these domains turn out to be the dominant source of the gravitational wave signal (see §S2). The existence of domain walls relies on there being a two dimensional field space. If the field space is higher dimensional, it is possible that higher dimensional transient defects like strings or textures will play a similar role.

The existence of transient h -domains (with accompanying domain walls) in this class of models is novel. The development of a non-zero ϕ vev was first pointed out in [15] and understood in terms of the initial backreaction of the resonantly produced h quanta on the ϕ condensate, but the existence of domain walls in such models was not discussed. Note that within $\Delta t \sim 10m_\phi^{-1}$, the domains disappear completely, and the fields enter a long turbulent stage. Perhaps, the shortness of the period in which the domains exist was the reason they were not noticed in [15].

At a more detailed level, we also monitored the power spectra of the two fields $P_F(k) \propto k^3 |F(k)|^2$ ($F = h, \phi$) to understand the distribution and time evolution of field perturbations at different scales (see Fig. S3). Note that the power spectra have been scaled by the the amplitude of the oscillating modulus. Thus when the spectra are of order unity, the rms fluctuations in the fields are becoming comparable to the background modulus field, signaling fragmentation of the modulus.

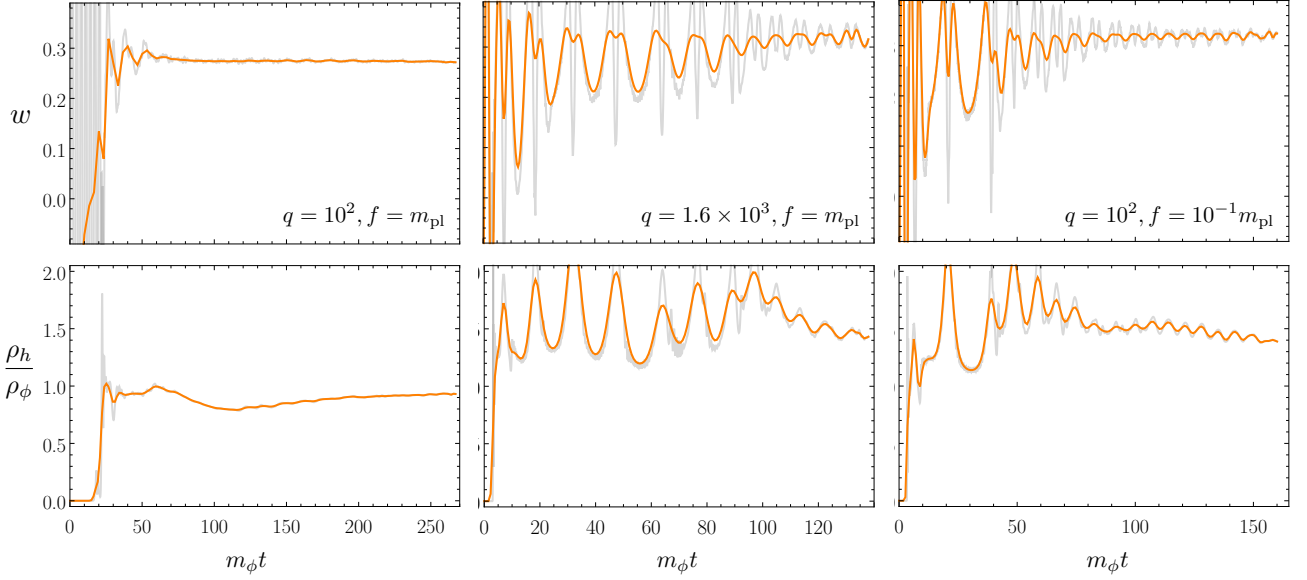


FIG. S4. The evolution of the equation of state, w , and the ratio of the mean Higgs and modulus densities, ρ_h/ρ_ϕ . After backreaction, for $qm_{\text{pl}}/f > 10^2$, there is a short-lived oscillatory phase. Despite this curious behaviour w settles to a constant value around 0.3. We have chosen parameters such that $b = 1$ in all cases. The grey and orange curves are obtained by averaging over space, with additional averaging over fast oscillations for the orange curves.

Along with the fields, we keep track of the spatially averaged energy density

$$\rho = \rho_\phi + \rho_h + \rho_{\text{int}}, \quad (\text{S12})$$

where

$$\rho_\phi = \frac{1}{2}\dot{\phi}^2 + \frac{1}{2}\left(\frac{\nabla\phi}{a}\right)^2 + \frac{1}{2}m_\phi^2\phi^2, \quad \rho_h = \frac{1}{2}\dot{h}^2 + \frac{1}{2}\left(\frac{\nabla h}{a}\right)^2 + \frac{1}{4}\lambda h^4, \quad \rho_{\text{int}} = \frac{1}{2}\frac{M^2}{f}\phi h^2, \quad (\text{S13})$$

as well as the pressure

$$p = \frac{1}{2}\dot{\phi}^2 + \frac{1}{2}\dot{h}^2 - \frac{1}{6}\left(\frac{\nabla\phi}{a}\right)^2 - \frac{1}{6}\left(\frac{\nabla h}{a}\right)^2 - \frac{1}{2}m_\phi^2\phi^2 - \frac{1}{2}\frac{M^2}{f}\phi h^2 - \frac{1}{4}\lambda h^4. \quad (\text{S14})$$

The equation of state is defined as $w \equiv \langle p \rangle / \langle \rho \rangle$ where the angular brackets include a spatial average and when there are rapid oscillations, a temporal average as well. In Figs. S4 and 3, we show the results for the evolution of the energy densities and the equation of state for a range of parameters. Note that for the results in Figs. S4, we have chosen parameters so that the fragmentation efficiency $b = 1$, but allowed other parameters to vary. For the cases considered, the equation of state after fragmentation always settles near $1/4 \lesssim w \lesssim 1/3$, and the amount of energy density in the modulus and Higgs fields are comparable.

S2 Gravitational Waves and Lattice Simulations

1. Equations of Motion

We calculate the gravitational waves generated by the nonlinear field dynamics using

$$\ddot{h}_{ij}^{TT} + 3H\dot{h}_{ij}^{TT} - \frac{\nabla^2}{a^2}h_{ij}^{TT} = \frac{2}{m_{\text{pl}}^2}\Pi_{ij}^{TT} \quad (\text{S15})$$

where h_{ij}^{TT} is the spatial, transverse, traceless part of the metric perturbations ($g_{\mu\nu} = g_{\mu\nu}^{\text{FRW}} + h_{\mu\nu}$), and Π_{ij}^{TT} is the transverse-traceless part of the energy momentum tensor of the fields which sources the gravitational waves. This is a “passive calculation” where the (small) backreaction of the metric perturbations on the fields is ignored.

2. Characteristic Scales

Let us consider a gravitational wave generated at $a = a_g$ in the early universe with a co-moving wavenumber k . By taking into account red-shifting due to expansion and conservation of entropy after thermalization, the frequency today of this GW signal is

$$f_0 = \frac{1}{2\pi} \frac{k}{a_0} = \frac{1}{2\pi} \left(\frac{k}{a_g H_g} \right) \sqrt{H_g H_0} \left(\frac{a_g}{a_{\text{th}}} \right)^{(1-3w_{\text{mod}})/4} \left(\frac{g_{\text{th}}}{g_0} \right)^{-1/12} \Omega_{\text{r},0}^{1/4}, \quad (\text{S16})$$

where H_g is the Hubble parameter of the universe at the time of generation of the gravitational waves, g_{th} and g_0 are the effective number of relativistic degrees of freedom at the epoch of thermalization (a_{th}) and today (a_0), $\Omega_{\text{r},0}$ is the fractional energy density in relativistic species today and w_{mod} is the mean equation of state between generation and thermalization (after which we assume a standard thermal history).

We can parametrize the characteristic wavenumber at which the gravitational waves are generated:

$$\frac{k}{a_g H_g} \equiv \beta^{-1} \sim q^{1/2} \frac{m_{\text{pl}}}{\sqrt{f\phi_g}}, \quad (\text{S17})$$

where the parameter β has been estimated from an analysis of the linear instabilities in the field perturbations (see eq. (S9)), with ϕ_g being the amplitude of the modulus at the time of GW production.

The fraction of energy density in gravitational waves per logarithmic interval in wavenumber today is conventionally given as $\Omega_{\text{gw},0} = \rho_{\text{c},0}^{-1} (d \ln \rho_{\text{gw},0} / d \ln k)$. Since GWs redshift as radiation, one can show that

$$\Omega_{\text{gw},0} = \Omega_{\text{gw}} \times \left(\frac{a_g}{a_{\text{th}}} \right)^{1-3w_{\text{mod}}} \left(\frac{g_{\text{th}}}{g_0} \right)^{-1/3} \Omega_{\text{r},0}, \quad (\text{S18})$$

where Ω_{gw} is the fractional energy density in gravitational waves at the time of generation. Ω_{gw} can be estimated using the characteristic wavenumber above and assuming that a fraction δ_π of the energy density is involved in generating the gravitational waves (see for example [23], with significant fragmentation, $\delta_\pi \lesssim 0.3$):

$$\Omega_{\text{gw}} = \frac{1}{\rho_g} \frac{d \ln \rho_{\text{gw}}}{d \ln k} \sim \beta^2 \delta_\pi^2, \quad (\text{S19})$$

where ρ_g is the total density at the time of generation of the gravitational waves. A more detailed discussion of such scalings (with slightly different parametrization) can be found [29].

For $g_{\text{th}}/g_0 = 10^2$, $H_0 = 1.4 \times 10^{-33}$ eV, $\Omega_{\text{r},0} = 6.4 \times 10^{-5}$ [30], we can get an estimate of the characteristic frequency and amplitude of the gravitational energy density:

$$f_0 \sim \beta^{-1} \sqrt{\frac{m_\phi}{10^5 \text{ TeV}}} \sqrt{\frac{\phi_g}{m_{\text{pl}}}} \left(\frac{a_g}{a_{\text{th}}} \right)^{(1-3w_{\text{mod}})/4} \times 10^5 \text{ Hz}, \quad (\text{S20})$$

$$\Omega_{\text{gw},0} \sim \beta^2 \delta_\pi^2 \left(\frac{a_g}{a_{\text{th}}} \right)^{(1-3w_{\text{mod}})} \times 10^{-5},$$

where $\beta^{-1} \sim q^{1/2} m_{\text{pl}} / \sqrt{f\phi_g}$. For the simulation parameters ($q = 10^2, b = 1, f = m_{\text{pl}}$) for Figs. 4 and S5, we get $\beta \sim 0.1$.

3. Lattice Simulations and Results

To calculate the GWs we use HLattice [24]. We calculate them passively, i.e., we evolve the metric perturbations without accounting for their feedback on the fields and metric dynamics. We use the 6th-order symplectic integrator for the self-consistent evolution of the fields and the scale factor, the HLATTICE2 spatial-discretization scheme and k_{eff} (not k_{std}) for the TT projector.

Figs. 4 and S5 are based on lattice simulations with $N = 256^3$, $L_{\text{in}} H_{\text{in}} = 2.0$ and $dt = L_{\text{in}} / (16N^{1/3}) \approx 0.00120 m_\phi$. The time step for the gravitational waves is $dt_{\text{GW}} = 4dt$. At the end of the simulation $a \approx 12$, which corresponds to $t \approx 70 m_\phi^{-1}$ (this is also the time when the equation of state settles to a constant value, see orange curve in Fig. 3).

The results of our simulations for gravitational waves are given in Fig. S5 (right). We show the time evolution of the gravitational wave spectra up to $t \approx 70 m_\phi^{-1}$. The initial tachyonic instability in the Higgs

generates GWs with well-defined cut-off, $f_0 \lesssim q^{1/2} \sqrt{m_\phi m_{\text{pl}} / (f \times 10^5 \text{ TeV})} 10^5 \text{ Hz} \approx 10^5 \text{ Hz}$, corresponding to the comoving modes $k < m_\phi q^{1/2}$. After backreaction, the spectrum settles down and GWs are slowly generated on intermediate frequencies, as power propagates towards smaller comoving scales, see Fig. S3.

In Fig. 4 in the main text, we scale the gravitational wave spectrum at $t \approx 70m_\phi^{-1}$ assuming different subsequent expansion histories characterized by $(N_{\text{mod}}, w_{\text{mod}})$. For the parameters $q = 100, b = 1, f = m_{\text{pl}}$, we found $\delta_\pi \sim 0.3$ and $\beta \sim 0.1$, showing a consistency between our estimates in the previous sub-section and the results of the numerical simulations.

A more detailed understanding of the main source of gravitational wave production is obtained by specifically considering the domain walls formed in the Higgs-modulus system as seen in Fig. S2. The GW power emitted by a single ‘bubble’ with quadrupole moment Q and radius R is (see [31])

$$P_{\text{gw,g}} \sim G \ddot{Q}^2 \sim G \left(\frac{R^5 \rho_{h,g}}{R^3} \right)^2, \quad (\text{S21})$$

where the subscript g denotes quantities at the time of generation of the GWs. We also have $P_{\text{gw,g}} \sim \rho_{\text{gw,g}} R^2$ from which follows that

$$\frac{\rho_{\text{gw,g}}}{\rho_{h,g}} \sim G \rho_{h,g} R^2. \quad (\text{S22})$$

At the time of domain formation $t_g \sim 22m_\phi^{-1}$, $\rho_{h,g} \lesssim \rho_{\phi,g} \lesssim \rho_g$ (where ρ_g is the total energy density in the fields at the time of generation of the GWs). From the simulations $R \sim 10m_\phi^{-1}$ (see second column in Fig. S2), implying

$$\Omega_{\text{gw,g}} \sim \left(\frac{\rho_{h,g}}{\rho_g} \frac{\rho_{\phi,g}}{\rho_g} \right) \frac{\phi_g^2}{m_{\text{pl}}^2} \sim 10^{-3}. \quad (\text{S23})$$

In the above estimate, we take the factor in the brackets to be $\sim 10^{-1}$ and $\phi_g \sim 10^{-1} m_{\text{pl}}$ consistent with simulations. This explains the strength of the signal $\Omega_{\text{gw},0} \sim \Omega_{\text{gw,g}} \times \Omega_{r,0} \sim 10^{-8}$.

In our model with two real fields, the formation of the transient domain walls is important for the generation of GWs, giving an order of magnitude stronger signal than the one from the subsequent long turbulent stage. The time of formation of the domains and their length scale properly accounts for peak in the gravitational wave spectrum. In a more realistic theory, with a complex Higgs and moduli fields along with gauge fields, it is possible higher dimensional transient textures to play a qualitatively similar role. We leave this investigation to future work.

S3 Inflationary Constraints The key point is that the e -folds between the time the current comoving horizon scale exited the horizon during inflation and the end of inflation are related to the e -folds between the end of inflation and today in a given expansion history. The expansion history also allows us to keep track of the evolution of the energy density. Then the n_s and r bounds from CMB measurements constrain an inflationary model together with its associated evolution afterwards. This basic idea was proposed in Ref. [27].

The cosmological history that we consider includes inflation, inflationary reheating characterized by a constant w_{re} in the equation of state, radiation domination, an early matter domination phase starting when $H \approx m_\phi$ and the modulus begins to oscillate around its minimum, and radiation domination again after the perturbative decays of modulus. Differing from the discussions in Ref [32–34], we include a possible non-trivial equation of state with a constant $w_{\text{mod}} \neq 0$ originating from non-perturbative particle production after the modulus starts to oscillate and before the full conversion of the modulus energy into radiation. The constant, w_{re} , could be taken as an average from the end of inflation till radiation domination and satisfies

$$\frac{\rho_{\text{rad}}}{\rho_{\text{end}}} = \left(\frac{a_{\text{end}}}{a_{\text{rad}}} \right)^{3(1+w_{\text{re}})}, \quad (\text{S24})$$

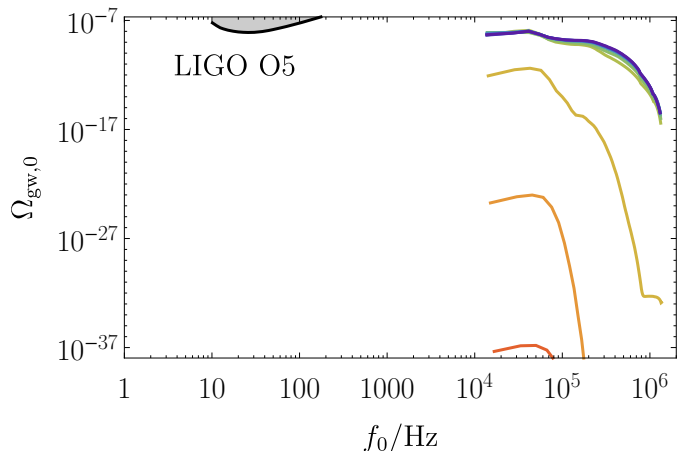


FIG. S5. The growth in the amplitude of the GW power spectrum from the end of inflation to $t \approx 70m_\phi^{-1}$ (with $b = 1, q = 10^2, f = m_{\text{pl}}$). The curves are output at time intervals $\Delta t = 6m_\phi^{-1}$.

where $a_{\text{end}}, a_{\text{re}}$ ($\rho_{\text{rad}}, \rho_{\text{re}}$) are the scale factors (energy densities) at the end of inflation and at the end of inflationary reheating respectively. Similarly, w_{mod} is the average from modulus oscillation till its full decay and satisfies

$$\frac{\rho_{\text{mod}}}{\rho_{\text{dec}}} = \left(\frac{a_{\text{dec}}}{a_{\text{mod}}} \right)^{3(1+w_{\text{mod}})}, \quad (\text{S25})$$

where $a_{\text{mod}}, a_{\text{dec}}$ ($\rho_{\text{mod}}, \rho_{\text{dec}}$) are the scale factors (energy densities) when the modulus starts to oscillate and when full decays of the modulus happen (equivalently when radiation dominates again) respectively.

Our derivation closely follows Ref [33] and we will summarize the key steps below. The comoving Hubble scale $k = a_k H_k$ that exits the horizon during inflation could be written as

$$k = a_k H_k = \frac{a_k}{a_{\text{end}}} \frac{a_{\text{end}}}{a_{\text{re}}} \frac{a_{\text{re}}}{a_{\text{mod}}} \frac{a_{\text{mod}}}{a_{\text{dec}}} a_{\text{dec}} H_k, \quad (\text{S26})$$

In terms of e -folds, $e^{N_k} = \frac{a_{\text{end}}}{a_k}$, $e^{N_{\text{re}}} = \frac{a_{\text{re}}}{a_{\text{end}}}$, $e^{N_{\text{RD}}} = \frac{a_{\text{mod}}}{a_{\text{re}}}$, $e^{N_{\text{mod}}} = \frac{a_{\text{dec}}}{a_{\text{mod}}}$, we have

$$\ln k = -N_k - N_{\text{re}} - N_{\text{RD}} - N_{\text{mod}} + \ln a_{\text{dec}} + \ln H_k. \quad (\text{S27})$$

Note that the e -folds between the modulus oscillation and full energy conversion into radiation is given by

$$N_{\text{mod}} = \frac{1}{3(1+w_{\text{mod}})} \ln \frac{\rho_{\text{mod}}}{\rho_{\text{dec}}}. \quad (\text{S28})$$

In addition, a_{dec} could be rewritten in terms of the scale factor, a_0 , today. Given the conserved comoving entropy, it can be achieved by relating the energy density at the end of modulus epoch, ρ_{dec} to the temperature today through

$$\rho_{\text{dec}} = \frac{\pi^2}{30} g_{\text{dec}} T_{\text{dec}}^4, \quad \frac{T_{\text{dec}}}{T_0} = \left(\frac{g_{0;s}}{g_{\text{dec};s}} \right)^{1/3} \frac{a_0}{a_{\text{dec}}}, \quad (\text{S29})$$

where $g_{\text{dec};s}$ and $g_{0;s}$ are the effective degrees of freedom for entropy. Furthermore, N_{RD} can be replaced by

$$\ln \rho_{\text{mod}} = \ln \frac{\rho_{\text{mod}}}{\rho_{\text{re}}} + \ln \frac{\rho_{\text{re}}}{\rho_{\text{end}}} + \ln \rho_{\text{end}} \quad (\text{S30})$$

$$= -4N_{\text{RD}} - 3(1+w_{\text{re}})N_{\text{re}} + \ln \rho_{\text{end}} \quad (\text{S31})$$

Combining all the equations above, we have

$$\begin{aligned} \frac{1-3w_{\text{mod}}}{4} N_{\text{mod}} &= -N_k - \frac{1-3w_{\text{re}}}{4} N_{\text{re}} \\ &+ \frac{1}{4} \ln \left(\frac{\pi^2}{30} g_{\text{dec}} \left(\frac{g_{0;s}}{g_{\text{dec};s}} \right)^{4/3} \right) - \ln k + \ln H_k - \frac{1}{4} \ln \rho_{\text{end}} + \ln(a_0 T_0) \end{aligned} \quad (\text{S32})$$

This equation relates the e -folds in the modulus epoch to the e -folds in the inflation epoch. For slow-roll inflation,

$$H_k^2 = \frac{\pi^2}{2} m_{\text{pl}}^2 r A_s = \frac{\rho_k}{3m_{\text{pl}}^2} \Rightarrow \ln H_k = \frac{1}{4} \ln \left(\frac{\pi^2 r A_s}{6} \right) + \frac{1}{4} \ln \rho_k, \quad (\text{S33})$$

where r is the tensor-to-scalar ratio, A_s the amplitude of scalar perturbation and ρ_k is the energy density when the mode exits the horizon. In addition, using

$$\left(\frac{a_{\text{dec}}}{a_{\text{mod}}} \right)^{\frac{3}{2}(1+w_{\text{mod}})} = 1 + \frac{3}{2}(1+w_{\text{mod}})H(t_{\text{mod}})(t_{\text{dec}} - t_{\text{mod}}), \quad (\text{S34})$$

N_{mod} could be expressed in terms of the modulus mass,

$$\begin{aligned} N_{\text{mod}} &\approx \frac{2}{3(1+w_{\text{mod}})} \ln \left(\frac{3}{2}(1+w_{\text{mod}})H(t_{\text{mod}})\tau_{\text{mod}} \right), \\ &= \frac{2}{3(1+w_{\text{mod}})} \ln \left(\frac{3}{2}(1+w_{\text{mod}}) \frac{m_{\text{pl}}^2}{c \times m_{\phi}^2} \right), \end{aligned} \quad (\text{S35})$$

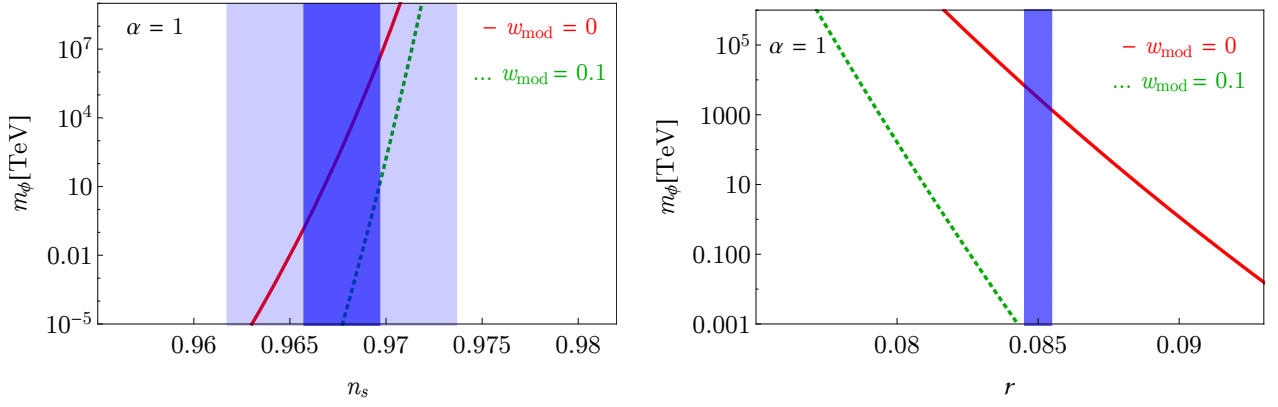


FIG. S6. The lower bound on m_ϕ as a function of n_s (left) and r (right) with the inflation model in Eq. S40 and $\alpha = 1$. The red solid and green dotted lines correspond to $w_{\text{mod}} = 0$ and 0.1 respectively. In the left panel, the light blue shaded region corresponds to the current 1σ bounds on n_s from Planck TT+lowP+lensing. The narrower darker blue shaded region corresponds to the 1σ bounds of a future CMB experiment of n_s with sensitivity $\pm 2 \times 10^{-3}$ [35], assuming the same central value as Planck. In the right panel, the blue shaded region corresponds to the 1σ bounds of a future CMB experiment of r with sensitivity $\pm 5 \times 10^{-4}$ [35], assuming a measured central value of r being 0.085.

where we approximated $t_{\text{dec}} - t_{\text{mod}}$ by the perturbative lifetime of the modulus $\tau_{\text{mod}} = (cm_\phi^3/m_{\text{pl}}^2)^{-1}$ and $H(t_{\text{mod}}) \approx m_\phi$. Putting Eq. (S32), (S33), (S35) together, we have

$$\begin{aligned} \frac{1-3w_{\text{mod}}}{6(1+w_{\text{mod}})} \ln \left(\frac{3}{2}(1+w_{\text{mod}}) \frac{m_{\text{pl}}^2}{c \times m_\phi^2} \right) &= -N_k - \frac{1-3w_{\text{re}}}{4} N_{\text{re}} \\ + \frac{1}{4} \ln \left(\frac{\pi^2}{30} g_{\text{dec}} \left(\frac{g_{0;s}}{g_{\text{dec};s}} \right)^{4/3} \right) - \ln \left(\frac{k}{a_0 T_0} \right) + \frac{1}{4} \ln \left(\frac{\pi^2 r A_s}{6} \right) + \frac{1}{4} \ln \left(\frac{\rho_k}{\rho_{\text{end}}} \right) \end{aligned} \quad (\text{S36})$$

$$= -N_k - \frac{1-3w_{\text{re}}}{4} N_{\text{re}} + 57 + \frac{1}{4} \ln r + \frac{1}{4} \ln \left(\frac{\rho_k}{\rho_{\text{end}}} \right), \quad (\text{S37})$$

where we use $\ln(10^{10} A_s) = 3.062$ (central value of Planck TT+lowP+lensing) at $k = 0.05 \text{ Mpc}^{-1}$ [30], $T_0 = 2.725 \text{ K}$, $g_{0;s} = 3.91$ and $g_{\text{dec};s} = g_{\text{dec}} = 10.76$. Thus we obtain a lower bound on m_ϕ ,

$$m_\phi^2 \gtrsim \frac{3(1+w_{\text{mod}})}{2c} m_{\text{pl}}^2 \exp \left(-\frac{6(1+w_{\text{mod}})}{1-3w_{\text{mod}}} \left(-N_k - \frac{1-3w_{\text{re}}}{4} N_{\text{re}} + 57 + \frac{1}{4} \ln r + \frac{1}{4} \ln \left(\frac{\rho_k}{\rho_{\text{end}}} \right) \right) \right) \quad (\text{S38})$$

Note that generically we expect $0 < w_{\text{re}} < 1/3$ and $(1/4)(1-3w_{\text{re}})N_{\text{re}} > 0$, which leads to a conservative bound on m_ϕ independent of the details of the inflation reheating stage

$$m_\phi^2 \gtrsim \frac{3(1+w_{\text{mod}})}{2c} m_{\text{pl}}^2 \exp \left(-\frac{6(1+w_{\text{mod}})}{1-3w_{\text{mod}}} \left(-N_k + 57 + \frac{1}{4} \ln r + \frac{1}{4} \ln \left(\frac{\rho_k}{\rho_{\text{end}}} \right) \right) \right). \quad (\text{S39})$$

The presence of a non-zero w_{mod} could change the bound on m_ϕ dramatically compared to the case with $w_{\text{mod}} = 0$. Since the logarithmic terms in the exponent in Eq. S38, S39 are usually tiny, a crude rule of thumb is that when $N_k < 57$, the bound could be significantly weakened with $w_{\text{mod}} > 0$ while when $N_k > 57.0$, the bound is more tightened with $w_{\text{mod}} < 0$. The details of the bounds depend on specific inflation models. Let's take a look at the model with a polynomial potential

$$V_{\text{inf}} = \frac{1}{2} m^4 \phi_{\text{inf}}^\alpha, \quad (\text{S40})$$

where ϕ_{inf} is the inflaton and $\alpha > 0$. In this case, N_k, r and ρ_k/ρ_{end} can be written in terms of the spectral index n_s and the power α :

$$N_k = \frac{\alpha + 2}{2(1 - n_s)}, \quad r = \frac{8\alpha(1 - n_s)}{\alpha + 2} \quad (\text{S41})$$

$$\frac{\rho_k}{\rho_{\text{end}}} = \frac{2}{3} \left(\frac{2(\alpha + 2)}{\alpha(1 - n_s)} \right)^{\alpha/2}. \quad (\text{S42})$$

In our evaluation below, we use $n_s = 0.9677 \pm 0.006$ (Planck TT+lowP+lensing) [30]. We also fix $c = 1/16\pi$. For $\alpha = 1$, the lower bounds on m_ϕ as a function of n_s or r are illustrated in Fig. S6. In this case, the central value of n_s gives us $N_k \approx 46.4, r \approx 0.086, \rho_k/\rho_{\text{end}} \approx 9$. This leads to a conservative lower mass bound of the modulus, $m_\phi > 477$ TeV when $w_{\text{mod}} = 0$ and a much weaker bound when w_{mod} increases, e.g., $m_\phi > 8$ MeV when $w_{\text{mod}} = 0.1$. Yet the potential strong mass bound on the modulus for $w_{\text{mod}} = 0$ may not be solid given the current precision of n_s . If we allow for n_s to vary in the 1σ range, for instance, when n_s takes the value at the lower 1σ bound, $n_s = 0.962$, $N_k \approx 39.2, r \approx 0.10, \rho_k/\rho_{\text{end}} \approx 8.3$. When $w_{\text{mod}} = 0$, $m_\phi > 0.14$ MeV, which is negligible. In the future, if the precision of n_s could be improved by a factor of 2 to 3 with the CMB-S4 measurements [35], we will have a better assessment of the compatibility of the modulus scenario and different classes of inflation models.

A more optimistic scenario is that in the near future, we will detect primordial gravitational waves and measure r . The precision of CMB-S4 measurement of r is projected to be significantly improved to 5×10^{-4} . Assuming a measured $r = 0.085$ and CMB-S4's sensitivity, we could obtain a solid lower bound on m_ϕ : $m_\phi > 1000$ TeV, when $w = 0$ as shown in the right panel of Fig. S6. When w is increased to 0.1, the bound is considerably relaxed to be well below the cosmological moduli bound.

S4 Aspects of the model

1. Fine tuning and duration of non-linear dynamics

In an *untuned* scenario, e.g., $\phi_0 \lesssim f$ in Eq. 1, at the beginning of the modulus oscillation, there is still a transition between the unbroken and broken electroweak phases, associated with tachyonic Higgs production. The initial fragmentation of the modulus and burst of gravitational waves are thus possible even in theories that are not fine-tuned. However, as the universe expands, the amplitude of the modulus oscillation quickly reduces. Once $|\phi(t)| < \phi_0$, the Higgs potential is always in the broken phase, so we expect that the coupled phase with exotic equation of state turns off and the system quickly returns to a standard moduli-dominated phase with $w \approx 0$. The bigger ϕ_0 is, the shorter the duration of the non-linear dynamics. In other words, the number of electroweak-flipping oscillations and hence the duration of non-linear dynamics is a probe of fine-tuning.

2. Origin of moduli couplings

In this section we will explain the origin of the $M^2(\phi/f)h^\dagger h$ ansatz for the modulus coupling to the Higgs, and some variations that can arise. We first start by supposing that the modulus is a chiral superfield $\mathbf{X} \supset X + F_X \theta^2$, with a supersymmetry breaking VEV

$$\langle \mathbf{X} \rangle = X_0 + F_{X,0} \theta^2, \quad \text{where } X_0 \sim m_{\text{pl}}, \quad F_{X,0} \sim m_{3/2} m_{\text{pl}}. \quad (\text{S43})$$

Generic chiral superfields will obtain soft SUSY-breaking mass terms through couplings to \mathbf{X} ,

$$\int d^4\theta \frac{\xi_{XZ}}{m_{\text{pl}}^2} \mathbf{X}^\dagger \mathbf{X} Z^\dagger Z \supset \xi_{XZ} \frac{|F_X|^2}{m_{\text{pl}}^2} Z^\dagger Z, \quad (\text{S44})$$

i.e. Z has a soft mass $\sim m_{3/2}^2$. If \mathbf{X} deviates from its vacuum expectation value, then in general this mass term will also fluctuate. For example, we might suppose that \mathbf{X} has a superpotential

$$W = \int d^2\theta \left(\frac{1}{2} m_X \mathbf{X}^2 + \frac{1}{3!} g_X \frac{m_X}{m_{\text{pl}}} \mathbf{X}^3 + \frac{1}{4!} \lambda_X \frac{m_X}{m_{\text{pl}}^2} \mathbf{X}^4 + \dots \right), \quad (\text{S45})$$

where $g_X, \lambda_X \sim \mathcal{O}(1)$ and factors of m_X/m_{pl}^{k-2} have been extracted to ensure that m_X acts as an overall spurion for shift-symmetry breaking. That is to say, it ensures that if $X \sim m_{\text{pl}}$ all terms in the potential are of comparable size. Now, if \mathbf{X} has a canonical Kähler potential $\int d^4\theta \mathbf{X}^\dagger \mathbf{X}$, then we can solve for the θ^2 component F_X as:

$$F_X^\dagger = \left(1 - \frac{\xi_{XZ}}{m_{\text{pl}}^2} Z^\dagger Z + \dots \right) \left(m_X X + \frac{1}{2} g_X m_X \frac{X^2}{m_{\text{pl}}} + \frac{1}{3!} \lambda_X m_X \frac{X^3}{m_{\text{pl}}^2} + \dots \right). \quad (\text{S46})$$

From this we see that requiring that X is the dominant source of SUSY breaking leads to $m_{3/2} \sim m_X$. This then parametrically guarantees that

$$F_X \sim m_{3/2} m_{\text{pl}} g(X) \quad (\text{S47})$$

where $g(X)$ is an order-one function of X/m_{pl} . In particular, the term (S44) contains a trilinear coupling:

$$\frac{2\xi_{XZ} \text{Re}(F_{X,0} m_X)}{m_{\text{pl}}^2} \text{Re}(X) Z^\dagger Z. \quad (\text{S48})$$

The prefactor here parametrically has size $m_{3/2}^2/m_{\text{pl}}$. This is the analogue of our toy model, with Z playing the role of the Higgs boson, $\text{Re}(X)$ playing the role of the modulus ϕ , and a prefactor of order M^2/f with $f \sim m_{\text{pl}}$ and $M \sim m_{3/2}$. In other words, a typical Planckian field displacement of X from its minimum will lead to an order-1 variation in the soft mass of Z .

We can also read off from this discussion that the $|F_X|^2$ term in the Lagrangian contains pieces that behave like

$$\frac{\xi_{XZ}^2 |m_X|^2}{m_{\text{pl}}^4} |Z|^4 |X|^2 (1 + \mathcal{O}(X/m_{\text{pl}}) + \dots). \quad (\text{S49})$$

In other words, we expect that moduli will inevitably generate quartic couplings of our fields with parametric size

$$\lambda_Z \sim \frac{m_{3/2}^2}{m_{\text{pl}}^2}. \quad (\text{S50})$$

Such F -term quartic couplings can also originate, as mentioned in the main text, from additional Kähler potential terms like $\int d^4\theta \frac{X^\dagger X}{\Lambda^4} (Z^\dagger Z)^2$. They will exist even, for instance, along D -flat directions of fields with gauge charges, as discussed in more detail below. The value of the quartic will be sensitive to the modulus value, but the parametric size will not.

In the context of the MSSM, moduli can affect Higgs soft masses by replacing $Z^\dagger Z$ with $\mathbf{h}_{u,d}^\dagger \mathbf{h}_{u,d}$, or they can affect holomorphic (b_μ -term) masses by coupling to $\mathbf{h}_u \mathbf{h}_d$. If the modulus primarily affects the b_μ -term rather than the soft masses, the dynamics can be rather different from our toy model, as a tachyonic direction exists both for large positive b_μ and for large negative b_μ , possibly disappearing in an intermediate region as the modulus oscillates. It would be interesting to simulate this scenario in future work.

Many theories of moduli have special points in field space where the metric is singular and a tower of particles becomes light, e.g. in string theory where many moduli fields T have Kähler potentials of the form $a \log(\mathbf{T} + \mathbf{T}^\dagger)$. Our field ϕ should be thought of as expanding around a value of $T \gg 1$, far from the singularity in moduli space at $T = 0$. The noncanonical Kähler term expanded around the minimum will give rise to terms like $\frac{1}{m_{\text{pl}}^2} \phi^2 \partial_\mu \phi \partial^\mu \phi$, which may influence the dynamics. We assume that the field remains far from the singularity at $T = 0$, so that it is valid to work in terms of the canonically normalized field ϕ . Nonetheless, as mentioned in §II, the omitted terms could have important dynamical effects. It would be interesting to include such terms in future simulations.

In general, working with moduli whose imaginary parts have associated shift symmetries, which appear via the combination $\mathbf{T} + \mathbf{T}^\dagger$, does not qualitatively change the discussion. In certain sequestered scenarios, couplings may take a different form. For example, in the context of the large-volume scenario, we expect that the SM matter fields are sequestered from the overall volume modulus and the leading modulus decay is from the coupling [36, 37]

$$\int d^4\theta \frac{\tilde{\mathbf{T}} + \tilde{\mathbf{T}}^\dagger}{\sqrt{3} m_{\text{pl}}} \mathbf{h}_u \mathbf{h}_d + \text{h.c.} \supset -\frac{1}{\sqrt{3} m_{\text{pl}}} (\square T) h_u h_d + \text{h.c.} \quad (\text{S51})$$

Here $\tilde{\mathbf{T}}$ is a modified chiral superfield missing its F -component, which is related to the conformal compensator in a superspace formulation of the theory [38]. In the presence of an oscillating solution $\square T \sim m^2 T$, this generates similar physics to a b_μ term linearly proportional to the modulus. After the modulus fragments, it could lead to rather different dynamics due to the derivatives acting on the modulus. Again, it could be interesting to simulate such variations in the future.

3. The potential along a D -flat direction

Supersymmetric theories with renormalizable superpotentials generically have a variety of flat directions [39, 40]. The flat directions of the renormalizable, supersymmetric MSSM, together with the leading non-renormalizable operators that lift them, have been catalogued in [41]. The existence of these flat directions is well known to have potential effects on cosmology, most famously for baryogenesis [42, 43].

Recall that in the MSSM, the tree-level Higgs mass matrix for the neutral modes $h_{u,d}^0$ takes the form

$$\begin{pmatrix} |\mu|^2 + m_{h_u}^2 & -b_\mu \\ -b_\mu & |\mu|^2 + m_{h_d}^2 \end{pmatrix}, \quad (\text{S52})$$

so it will have a tachyonic eigenvalue if one of the soft terms $m_{h_{u,d}}^2$ is sufficiently negative or if b_μ is sufficiently large (with either sign). We expect that in a sufficiently general theory, all of these terms will depend on the value of the modulus, so it oscillations can produce tachyons of either type (soft mass-driven or b_μ -driven). There is a tachyonic SUSY-breaking mass along the supersymmetric D-flat direction $|h_u| = |h_d|$ when

$$m_{h_u}^2 + m_{h_d}^2 + 2|\mu|^2 - 2|b_\mu| < 0. \quad (\text{S53})$$

This condition could arise dynamically as the modulus oscillates in many models, for instance those in which the b_μ -term is driven by the ϕ oscillation. The condition may be especially easy to realize in models with an approximate shift symmetry that ensures $\tan\beta = 1$ at tree level [44–46], though this is not a necessary precondition. One might expect this tachyonic direction to be lifted by loop corrections; for example, there is a potential along the D-flat direction from one loop diagrams with tops or stops,

$$V_{1\text{-loop}} \approx \frac{3y_t^4}{16\pi^2} (h_u^\dagger h_u)^2 \left[\log \frac{m_{\tilde{t}}^2}{m_t^2} + \frac{X_t^2}{m_t^2} \left(1 - \frac{1}{12} \frac{X_t^2}{m_t^2} \right) \right]. \quad (\text{S54})$$

However, it is important to note that the masses $m_{\tilde{t}}$ and m_t in this formula themselves depend on the value of the Higgs field, e.g. $m_{\tilde{t}}^2 \approx y_t^2 |h_u^0|^2 + \tilde{m}_{Q_3, \bar{u}_3}^2$. At large values of the Higgs, EWSB contributions to the stop and top masses dominate over SUSY-breaking contributions and $\log \frac{m_{\tilde{t}}^2}{m_t^2} \sim m_{\text{soft}}^2 / |h|^2 \ll 1$. Effectively, far out along the flat direction supersymmetry is approximately restored in the sector of particles with large interactions with the Higgs boson. We can simply integrate them out, and the Higgs will behave as an approximate modulus with large field range. Similar results were discussed in [47] in a finite-temperature context, where the presence of exponentially large values of MSSM fields in the early universe was argued to solve the monopole problem. (For a related discussion of zero-temperature physics, see the “inverted hierarchy” [48].)

As is familiar from the Affleck-Dine mechanism, what will actually prevent the Higgs fields from taking arbitrarily large values along the flat direction are higher dimension operators.⁶ We can obtain quartic couplings along the flat direction from Kähler operators, for instance

$$\int d^4\theta \frac{\mathbf{X}^\dagger \mathbf{X}}{m_{\text{pl}}^4} (\mathbf{h}_u^\dagger \mathbf{h}_u)^2 \rightarrow \frac{|F_{X,0}|^2}{m_{\text{pl}}^4} (h_u^\dagger h_u)^2. \quad (\text{S55})$$

This gives an effective quartic

$$\lambda \sim \frac{m_{3/2}^2}{m_{\text{pl}}^2}, \quad (\text{S56})$$

which is precisely what is needed to give a fragmentation efficiency $b \sim 1$, assuming $m_\phi, M \sim m_{3/2}$ and $f \sim m_{\text{pl}}$.

At first glance it appears that superpotential terms can prevent such large field values. For example, a superpotential

$$\int d^2\theta \left(\mu \mathbf{h}_u \mathbf{h}_d + \frac{1}{M_*} (\mathbf{h}_u \mathbf{h}_d)^2 \right) \quad (\text{S57})$$

gives rise to quartic terms such as

$$\frac{\mu^\dagger}{M_*} (h_u^\dagger h_u) (h_u h_d) + \text{h.c.}, \quad (\text{S58})$$

⁶ In some cases, radiative effects will cause the tachyonic eigenvalue along the D-flat direction to run positive at values of the Higgs field well below the cutoff. It is then important to compute a

renormalization group-improved effective potential. JF and MR thank Prateek Agrawal for useful conversations on this point, which we hope to explore in more detail elsewhere.

which would stop the Higgs along the flat direction at values of order $(\mu M_*)^{1/2}$. If we take $M_* \sim m_{\text{pl}}$, these are small field values and we would never achieve a sufficiently large fragmentation efficiency. However, any realization of the MSSM should contain a solution to the μ problem, explaining why the coefficient of $\int d^2\theta \mathbf{h}_u \mathbf{h}_d$ is much smaller than the Planck scale. We expect that such a solution will generically imply that higher order superpotential terms like $\int d^2\theta (\mathbf{h}_u \mathbf{h}_d)^2$ also have parametrically small coefficients related to the same spurion μ/m_{pl} . Provided that $1/M_* \lesssim \mu/m_{\text{pl}}^2$, we obtain a sufficiently small quartic.

Since this spurion argument is rather abstract, let us consider a more explicit example of the expected size of the Higgs quartic coupling in the context of a particular solution of the μ problem. The Giudice-Masiero mechanism [49] invokes a Kähler term $\int d^4\theta \left(\frac{c_\mu}{m_{\text{pl}}} \mathbf{X}^\dagger \mathbf{h}_u \mathbf{h}_d + \text{h.c.} \right)$ which, if the F -component of \mathbf{X} obtains a VEV, becomes an effective superpotential μ -term with size of order soft SUSY-breaking parameters. For this mechanism to work, it is necessary that the true μ -term $\int d^2\theta \mu \mathbf{h}_u \mathbf{h}_d$ be highly suppressed or altogether absent from the superpotential. Although one can invoke the supersymmetric nonrenormalization theorem to excuse this assumption as technically natural, a better approach is to invoke a symmetry explanation (approximate or exact, discrete or continuous). For example, concrete completions of the Giudice-Masiero mechanism invoking discrete, anomaly free R -symmetries exist [50, 51]. As a simple example, the \mathbb{Z}_4 R -symmetry under which the superpotential has charge 2, the matter fields $\mathbf{q}, \bar{\mathbf{u}}, \bar{\mathbf{d}}, \ell, \bar{\mathbf{e}}$ have charge 1 and the Higgs fields $\mathbf{h}_{u,d}$ have charge 0 suffices to forbid a μ -term and enforce matter parity for proton stability. Notice that this symmetry forbids not only the μ -term itself but also higher-dimension operators such as $\int d^2\theta \frac{1}{\Lambda} (\mathbf{h}_u \mathbf{h}_d)^2$ that could affect the Higgs quartic coupling. In the context of this \mathbb{Z}_4 symmetry, we will encounter terms like

$$\int d^4\theta \frac{c_{\mu,2}}{m_{\text{pl}}^3} \mathbf{X}^\dagger (\mathbf{h}_u \mathbf{h}_d)^2 \rightarrow \int d^2\theta \frac{c_{\mu,2} F_{X,0}^\dagger}{m_{\text{pl}}^3} (\mathbf{h}_u \mathbf{h}_d)^2, \quad (\text{S59})$$

an effective superpotential quartic term with coefficient $\sim \frac{\mu}{m_{\text{pl}}^2}$. In other words, if the role of Giudice-Masiero is to suppress the μ term relative to the Planck scale by a small spurion μ/m_{pl} , the discrete symmetry approach ensures that the quartic Higgs superpotential term is suppressed by the same small spurion.